J Comput Aided Mol Des (2006) 20:511–518
DOI 10.1007/s10822-006-9069-8

GPCR SYMPOSIUM

Computational photochemistry of retinal proteins

Marius Wanko · Michael Hoffmann · Thomas Frauenheim · Marcus Elstner

Received: 8 June 2006 / Accepted: 18 August 2006 / Published online: 17 October 2006

Abstract High spectral tunability and quantum yield are the striking features of rhodopsin photochemistry. They rely on a strong and complex interaction of their chromophore, the protonated Schiff base of retinal, with its protein environment. In this article, we review the progress in the computational modeling of these systems, focusing on the optical properties and the excited state dynamics. While the earlier success of atomistic theoretical models was based on the breakthrough in X-ray crystallography and combined quantum mechanical molecular mechanical (QM/MM) methodology, recent advances point out the importance of high-level QM methods and the incorporation of effects that are neglected in conventional QM/MM or ONIOM schemes, like polarization and charge transfer.

Keywords Retinal · Rhodopsin · Color tuning · Opsin shift · Photoisomerization · QM/MM · MRCI · TDDFT · OM2 · SORCI

Abbreviations

B3LYP	Becke-3-parameter hybrid exchange and Lee–Yang–Parr correlation functional
BLA	Bond length alternation
bR	Bacteriorhodopsin
CASSCF	Complete active space self consistent field method
CASPT2	Complete active space method with second order perturbation correction
CCSD	Coupled cluster singles doubles
CHARMM	Chemistry at HArvard molecular mechanics
(TD)DFT	(Time-dependent) density functional theory
GGA	Generalized gradient approximation
HBN	Hydrogen bonded network
HF	Hartree–Fock method
LDA	Local density approximation
MP2	Second order Møller–Plesset perturbation theory
MRCI	Multi-reference configuration interaction
OM2	Orthogonalization method 2
PA	Proton affinity
ppR	Pharaonis phoborhodopsin (also called sensory rhodopsin II)
PSB	Protonated Schiff base
QM/MM	Combined quantum mechanical molecular mechanical method
SCC-DFTB	Self-consistent charge density functional based tight binding method
SORCI	Spectroscopy oriented configuration interaction

M. Wanko · M. Hoffmann · T. Frauenheim
BCCMS, Universität Bremen, Bremen 28334, Germany

M. Elstner
Theoretische Chemie, TU Braunschweig, Braunschweig 38106, Germany

M. Elstner (✉)
Department of Molecular Biophysics, German Cancer Research Center, Heidelberg 60120, Germany
e-mail: m.elstner@tu-bs.de

Introduction

Rhodopsins are membrane proteins that contain the molecule retinal as their chromophore, which triggers

the response of the cell to light. For example, in bacteriorhodopsin (bR), absorption of a photon leads to an all-*trans* to 13-*cis* isomerization of the retinal, which induces a proton transfer from the cytoplasmic to the extracellular side of the cell membrane. In rhodopsin, a member of the superfamily of G-protein coupled receptors, the photoabsorption invokes an 11-*cis* to all-*trans* isomerization, which puts the protein in its signaling state.

The retinal chromophore is covalently linked to the apoprotein via a protonated Schiff base. The protein environment drastically modulates the absorption maximum of the chromophore: while it is at about 450 nm in organic solvents [1], it varies from 360 to 635 nm in the light sensitive cone pigments [2], which are responsible for color vision. The question, how distinct protein environments regulate the maximum absorption (spectral tuning) of the retinal chromophore, is therefore a key question for understanding color vision.

Color tuning is achieved in nature by replacing certain amino acid residues, which can be simulated in mutation experiments. Mutations can yield very different effects, they can change (1) the protein electrostatic field by substituting charged or polar amino acids, (2) the protein polarizability by changing polarizable residues, and (3) introduce or remove steric interactions or induce structural changes by substituting small versus bulky residues. Three principal mechanisms for the color tuning have been identified [3]: (a) coplanarization of the ring-chain system and further distortion of the chromophore structure [4–8]; (b) electrostatic interaction of the chromophore with ionic, polar, and polarizable groups of the protein environment [9–12]; and (c) a change in the interactions between the chromophore and its complex counterion [13–15].

In any particular case, the detailed mechanism of color tuning is difficult to unravel experimentally, a predictive computational approach is therefore of great interest. Any theoretical approach, however, starts with the choice of structural and computational models, and is characterized by several modeling decisions:

- High resolution crystal structures are the starting point, and most modeling approaches differ in the treatment of the chromophore environment. Recent approaches use QM/MM schemes to incorporate the whole protein in the calculation, extending earlier attempts which focused on a model of the active site only (e.g., [16]). Definitely, the large impact of the protein electrostatics on the chromophore makes the inclusion of the whole protein necessary, the use of small parts of the protein active site may not lead to a successful model in general.
- On the other hand, most recent QM/MM calculations included only the chromophore into the QM region, leaving the remainder of the protein in the MM region. This choice neglects the effects of charge transfer, protein polarization, and dispersion interaction.[1]
- Only very few attempts to include the effects of solvation and lipid membrane have been reported [17]. It is not clear, up to now, to which extent an explicit, atomistic representation of the environment is necessary, or to which degree these effects can be incorporated by using continuum electrostatic approaches like the Poisson–Boltzmann (charge scaling) procedure [18].
- There are two approaches to the calculation of absorption energies: the first one is to use geometry-optimized QM/MM structures for single excitation energy evaluations [16, 19–21], the second is to sample the excitation energies along QM/MM MD trajectories [17, 22]. While for the first approach QM methods like DFT, HF, MP2, or even CASSCF have been used, the second approach needs fast QM methods like the semi-empirical MNDO, AM1, PM3, or EVB methods or the approximate DFT method SCC-DFTB. These methods are about three orders of magnitude faster than DFT or HF methods.
- QM methods vary substantially in their ability to accurately model the ground and excited states properties of the chromophore. Some methods fail completely, as e.g., the time-dependent DFT methods for retinal's excited states. It is therefore crucial to assess the QM methods for this particular system.

Nearly every attempt to calculate retinal absorption energies uses a different combination of the above listed ingredients, leading to a widespread range of data (since nearly every factor has some distinct impact on the excitation energy). Therefore, unless all factors are well controlled, a good agreement with experimental data can be due to a fortuitous cancelation of errors, which may or may not apply to one or the other rhodopsin.

The electronic ground state

Accurate calculations of retinal's ground-state properties are challenging for QM methods due to its highly

[1] Which partially have been included in earlier cluster models.

correlated and extended π-system. Therefore, we have tested various methods in some detail [23, 24], with respect to certain parameters that are critical for the modeling of ground- and excited-state processes. These are the bond length alternation (BLA), torsional barriers, and proton affinities, for the (gas-phase) relaxed structure but also for twisted conformations. The BLA, since it correlates with absorption energies and C=C stretch frequencies, as e.g., measured in Raman spectra of the chromophore. The torsional barriers, since they determine the degree of twisting of the chromophore due to the external forces in the binding pocket. The proton affinities, since they are crucial for the protonation state of the chromophore, i.e., proton-transfer reactions.

In [23] we showed that MNDO, AM1, and PM3 exhibit large quantitative errors, in particular for the torsional barriers, leading to a too flexible chromophore, which can be distorted too easily due to steric forces in the binding pocket [23]. DFT methods reproduce torsional barriers quite well, however, they vary in the description of the BLA. Pure DFT methods tend to underestimate the BLA, while HF and CASSCF severely overestimate it compared to MP2 and CASPT2. In [24] we showed that calculated excitation energies on HF-optimized chromophore geometries are biased, the error being as high as 0.4 eV within the protein environment. Hybrid HF-DFT methods like B3LYP exploit an effective error cancelation and yield reasonable geometries, the same holds for the SCC-DFTB method [25]. A good choice for QM/MM geometry optimization in the ground state is therefore made with the methods B3LYP, PBE0, MP2, and SCC-DFTB, where the latter can also be applied in extended QM/MM MD simulations (see below). In particular, SCC-DFTB has been applied lately to refine the rhodopsin crystal structure [26].

Methods that incorporate static but not dynamic correlation tend to overemphasize the dominant resonance in the valence bond structure, leading to overestimated charge localization and BLA. Density functionals on the LDA/GGA level, in opposite, tend to delocalize excess charges in extended conjugated systems and underestimate the BLA. The charge delocalization originates from the same deficiency of the exchange functional that leads to overestimation of polarizabilities and hyperpolarizabilities in extended conjugated chains [27, 28]. In the case of the PSB of retinal, it leads to an exaggerated stabilization of the proton at the Schiff base, i.e., to too large proton binding energies: while DFT is known to predict very accurate PAs for small molecules, it tends to fail, when

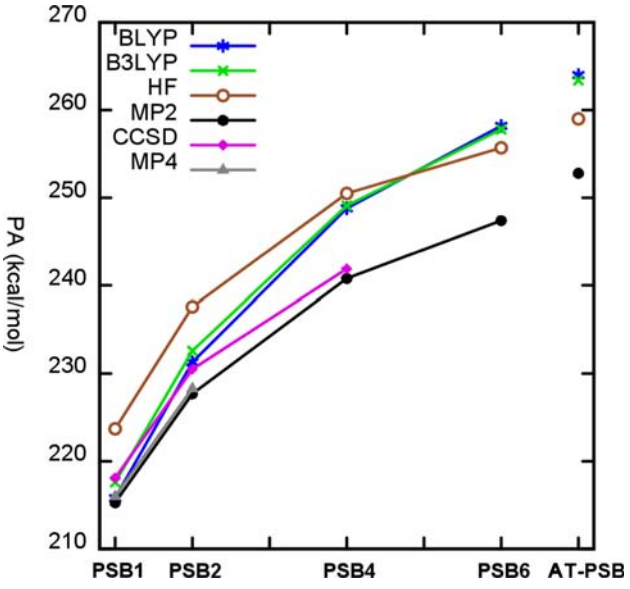

Fig. 1 Proton affinities of retinal models and all-*trans*-PSB. PSB*n* refers to a model with *n* conjugated double bonds. The employed basis set is TZVP for the SCF methods. The CCSD, MP2, and MP4 calculations employed the cc-pVTZ basis set and were performed on MP2/6-31G* optimized geometries

the positive charge of the proton can be delocalized in an extended π-system, as in retinal.

To illustrate this effect in more detail we show in Fig. 1 the PAs of retinal models, consisting of the Schiff base group, connected to polyene chains with one to six double bonds, i.e., of $NH_2^+=(C–C=)_nCH_2$, with $n = 0, \ldots, 5$. The MP2/cc-pVTZ data represent a fair reference for the other methods because the error of the MP2 method and the cc-pVTZ basis set partially cancel. For the PSB4 model, e.g., the coupled cluster singles doubles (CCSD) value is 1.1 kcal/mol higher in energy, while the basis set limit[2] of MP2 is 2.1 kcal/mol lower than the MP2/cc-pVTZ result. While B3LYP, BLYP, MP2, and CCSD agree for PSB1, they deviate considerably with increasing number of double bonds, leading to a PA overestimation of about 9 kcal/mol for the full chromophore.[3] Therefore, the application of DFT to proton transfer reactions in retinal proteins is not straightforward and should be pursued with some care [30]. In previous work on the first proton transfer step in bR, we have used either SCC-DFTB with specially calibrated parameters, or a DFT method

[2] The basis set limit of the MP2 PAs for the PSB6 model is extrapolated from the results of cc-pVTZ, cc-pVQZ, and cc-pV5Z calculations using the Schwartz formula [29].

[3] Note, that HF besides a systematic overestimation due to the lack of dynamic correlation shows the same length-dependency as the post-HF methods.

exploiting error cancelation by using restricted basis sets [30–32].

Absorption maximum and color tuning

Motivated by the large spectral shift of 71 nm on the one hand and their high degree of homology on the other, the spectral shift between bR and ppR has been addressed by various experimental and theoretical studies. Fixing the role of the mechanisms (a)–(c) in these proteins and their quantitative contribution to the shift has proven difficult, and many opposing models have been proposed. One reason for this controversy is the difficulty to separate the effects, e.g., in mutation experiments, where changes in the electrostatic environment of the chromophore are coincident with structural changes due to the mutation. Another is the fact that the QM methods employed in the theoretical models respond very differently to these tuning channels. Concerning mechanism (a), TDDFT displays the opposite trends than explicitly correlated methods: coplanarization, which can be regarded as effectively extending the length of the conjugated system, increases the TDDFT excitation energy, whereas smoothing the BLA blue-shifts it, in opposite to results of higher level methods. The change of the absorption maximum due to an external electric field, as generated by the counterion or other charged or polar residues, mechanism (b) and (c), is primarily caused by the Coulomb interaction between the external charge distribution and the difference dipole moment originating from the considerable charge transfer along the chromophore backbone as the latter is excited into the S_1 state. Also this effect is rendered differently by the various QM methods, ranging from strongly underestimating the effect (TDDFT, CIS) to overestimating it by a factor of two (CASSCF) [24]. This disagreement is related to the different degree of charge localization and charge transfer in the different QM methods, as mentioned above.

Derived from the assessment of methods for their ability to yield accurate shifts induced by the individual tuning factors, we suggested a computational strategy to obtain most unbiased and reliable absorption energies for retinal proteins within the framework of QM/MM [24]. The entire chromophore and the lysine side chain to which it is covalently bound are described by SCC-DFTB [25] for ground state properties and the semiempirical OM2/MRCI method [33] and ab initio SORCI method [34] for excited-state calculations. The remainder of the protein is modeled using the CHARMM force field. The QM and the MM region are connected via a link atom scheme, and interact both sterically and electrostatically. This methodology is efficient enough to afford studies of a wide variety of aspects, including dynamical effects. In our recent publication [35], we applied this scheme to analyze the spectral shift between bR and ppR. The calculated shift, based on QM/MM-optimized structures, agrees very well with the experiment (see Table 1), for the SORCI result as well as for the OM2/MRCI one.

We find that numerous sources contribute to the spectral shift between bR and ppR. The two main and equally important factors, which are responsible for about 90% of the total shift, are the different neutral amino acids in the binding pocket [mechanism (b)] and the difference in the extended hydrogen bonded network at the extracellular side of the proteins [mechanism (c)]. Differences in the chromophore geometries are small, and consist primarily in an increased BLA in ppR compared to bR, which again is induced by the electrostatic environment. Therefore, mechanism (a) plays only a minor role, contributing ca. 10% to the shift.

The chromophore is differently polarized by the polar and charged groups of the bR and the ppR protein environment. This is reflected in the change of the dipole moment with respect to vacuum $|\mu_{S_0}^{protein} - \mu_{S_0}^{vaccum}|$ and in the BLA along the polyene chain. Both, the BLA and the change of the dipole moment are clearly smaller in bR than in ppR, indicating a stronger electrostatic interaction with the protein in the latter.

Mutation experiments help to analyze the influence of distinct parts of the protein on the shift. Based on our theoretical model described above, we use two techniques to analyze the influence of single amino acids: a *perturbation analysis* displays the electrostatic effect of each amino acid on the excitation energy by repeating the excited-state calculation, with its side chain charges excluded. The second analysis simulates the mutation of one or several amino acids in one protein to their counterpart in the other protein.

Experimental mutation studies [38–42] identified several sites (e.g., Thr204Ala, Gly130Ser, Val108Met, Ala131Thr) in the binding pocket which have a

Table 1 Vertical excitation energies (eV) of bR and ppR

Method	bR	ppR	ΔE_{ppR-bR}
OM2/MRCI[a]	2.66	2.96	0.30
SORCI[a]	2.34	2.63	0.29
Experiment[b]	2.18	2.50	0.32

[a] From referene [35], [b] [36, 37]

significant impact, but none of them dominates the shift. Our simulations confirm these findings, and reveal some additional sites (by perturbation analysis) of smaller influence (e.g., Ala111Thr, Ser44Pro) outside the binding pocket, which have not been studied experimentally yet. Nevertheless, the interaction with all polar residues of the binding pocket accounts only for about 50% of the observed spectral shift. Experimental and our theoretical analyses of multiple mutants, e.g. the ppR mutant ''bR/ppR'' [41], with a binding pocket identical to that of bR, emphasize this fact.

The interaction of the counterion residues with the chromophore strongly depends on their distance [14, 15] from the Schiff base but also on other charged and polar groups that are connected to the HBN. Therefore, the discussion of this tuning mechanism focuses on the structure of the counterion complex and the three water molecules connecting the Schiff base and the counterion residues (extended HBN). The structural differences between bR and ppR mainly concern the different orientation of the guanidinium group of Arg82/72 and a distortion of the pentagonal cluster, formed by the two aspartic acids of the counterion complex and the three water molecules [43], in ppR (Fig. 2).

We have determined the influence of the extended HBN and further residues from the extracellular site (Glu204 for bR, Asp193 for ppR) to the spectral shift between bR and ppR by excluding the point charges of the remainder of the protein. Corresponding to our estimate, the entire counterion complex contributes 40–50% to the spectral shift between bR and ppR.

Although the results of our bR–ppR study are convincing and consistent with the available experimental findings, there are several effects that are neglected in the QM/MM schemes commonly used. The representation of the protein environment by fixed atomic charges neglects its static and dynamic polarizability and inter-residual charge transfer. The importance of static polarization has been emphasized for the dielectric screening of ionic groups [22] as well as for the response to the charge transfer on the chromophore during excitation [44]. The resulting effect on the excitation energy was estimated by using explicit polarization models, yielding red shifts from 0.34 to 0.19 eV [22, 44].

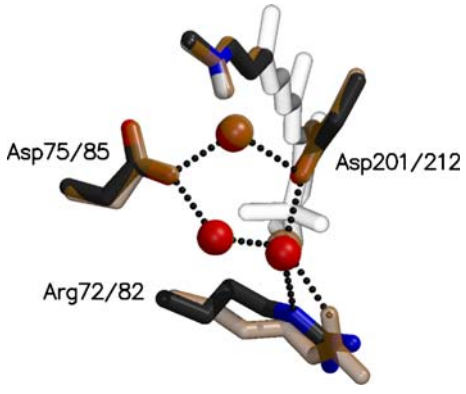

Fig. 2 Hydrogen bonded network of bR (1C3W, in brown/transparent) and ppR (1H68)

Motivated by these results, we applied an atomic polarization model, which overcomes some deficiencies of the former models. It includes the mutual interaction between the induced dipoles, and features a variational energy expression. The first is important for reproducing the non-isotropic polarizabilities of extended side chains (see Table 2) and cooperative effects while the latter leads to polarization energies that reproduce ab initio results. Since the fixed CHARMM force field charges incorporate polarization implicitly ''polarization-free'' charges are required to avoid double counting. We derived these from the electrostatic potential of the amino acid side chains in the gas phase.

In addition, we implemented a QM1/QM2/MM scheme, in which the polarization of the binding pocket (301 atoms) is treated on the DFT (QM2) level of theory. The charge distributions on the chromophore (QM1 = SORCI) and in the QM2 region are determined self-consistently by iterative calculations. Preliminary results, obtained with DFTB as QM2 method, indicate that the red shift with respect to the conventional QM/MM result is smaller than the previously predicted polarization shifts (Table 3). The QM1/QM2/MM model is in agreement with our empirical polarization model, which yields a corresponding shift of 0.1 eV.

A further project aims at including the dispersion and charge-transfer effects by extending the region included in the SCF or MRCI treatment. We find that in particular charge transfer from the chromophore to the counterions, across the HBN, affects the excitation energy, causing blue shifts of about 0.15 eV in bR and

Table 2 Polarizability (Å^3) of the tryptophane side chain calculated with our polarization model and SCF methods

Method	α_x	α_y	α_z	α
Additive	17.5	17.5	17.5	17.5
Interactive	18.9	17.3	9.4	15.2
HF	20.3	17.2	8.4	15.3
PBE0	21.4	17.8	8.4	15.9
PBE	22.1	18.2	8.5	16.3

Table 3 Excitation energies (eV) from the QM1/QM2/MM model for bR

QM1	QM2	MM	$\Delta E_{S_1-S_0}$
OM2/MRCI	CHARMM	CHARMM	2.67
OM2/MRCI	DFTB	CHARMM	2.60

QM1 contains the full chromophore and lysine side chain, QM2 contains 301 atoms of the binding pocket side chains, and MM contains the remainder of the protein

ppR. The dispersive interaction between the chromophore and adjacent aromatic groups differs in the ground and excited states, giving rise to bathochromic shifts in the excitation energies. This effect, well known from solvent shifts of non-polar solutes in non-polar solvents, can be estimated by empirical formulas derived from perturbation theory. Beside other approximations, these formulas assume an interaction between induced point dipoles. Since the separation between the chromophore and three aromatic residues is smaller than the dimension of the chromophore itself, this approximation is badly justified. An explicit, non-empirical description of the effect can be achieved by including these residues in the MRCI calculation. This is very costly and has been done only in a limited CI calculation on the semi-empirical level [16]. Using the SORCI method, an appropriate description of the dispersion interaction with all three aromatic residues is possible by including the required double excitations of the multi-configurational reference wave function. The results of these calculations will be published elsewhere.

The excited state photodynamics

From fs-spectroscopy studies of free and locked PSB retinal it is known that the excited state dynamics of rhodopsins is strongly modified by the protein environment. Compared with the decay of the fluorescent state (FS) in solution, which takes place on a time scale of <10 ps, excited state decay in the protein proceeds along a highly selective and efficient photoisomerization pathway. The latter can be blocked by locking the isomerizing double bond, resulting in a FS lifetime that is increased by several orders of magnitude whereas decay in solution is hardly changed. While in rhodopsin the photoisomerization on a 200 fs time scale was early established [45], the decay process and the time scale of isomerization and formation of the photoproduct in bR are still under debate [46–49].

Dynamical simulations of the full chromophore have until now not been achieved because of the high level of quantum methods that is required to correctly describe the excited state potential energy surface (as for the spectral tuning, DFT-based methods are not applicable [50]) and the need for nonadiabatic approaches, which take into account the strong coupling of adiabatic states in the intersection region. Further, the complexity of the protein interaction with the chromophore requires the inclusion of a large part of the binding pocket in the dynamical model.

The basic mechanism of the photoisomerization reaction and the factors that may determine the efficiency, bond selectivity, and time scale have been studied on the basis of model chromophores in the gas phase using the CASSCF/CASPT2 methodology [51–60]. After populating the S_1 state, BLA is inverted in the isomerizing region, which opens a barrierless path along double-bond torsional modes to the conical intersection (CI) seam. Studies on the CI seam have shown that the crossing is achieved by hydrogen pyramidalization rather than dihedral distortion of the carbon backbone [60], but since the first facilitates the latter, surface hopping MD simulations of the minimal *cis*-PSB3 model find highest hopping probability at 60–80° dihedral twist and decay to the ground state at the first approach of the crossing region within 50–80 fs [52, 60]. Both, the truncation of the chromophore's π-system and the use of CASSCF [58] increase the excitation energy at the FC point, and the potential energy surface slopes too steeply towards the conical intersection, which leads to an artificial acceleration of the excited state dynamics.

First attempts to simulate the photodynamics in bR have been presented, using very approximate QM models for the chromophore [22, 61]. Hayashi et al. [61], for example, applied CASSCF surface hopping to a PSB3 model, incorporating the remaining part of the chromophore as well as the protein environment of bR with an empirical force field. Despite the limitations of the QM part of the model, agreement of several features with experiment is achieved. After excitation, the chromophore relaxes along the C=C stretch modes and a species with red-shifted emission, reminiscent of the I460 intermediate, is formed, which decays in an incoherent way. The bond selectivity could be reproduced and the time scale of isomerization is significantly increased compared to the gas phase PSB3 model. Another shortcoming of this model, beside the truncated QM region, is its nonadiabatic dynamics scheme, which lacks a well defined hopping criterion, coherent propagation in the ground state, and an appropriate statistics to represent the full phase-space and sample the quantum mechanical expectation value for the ion forces.

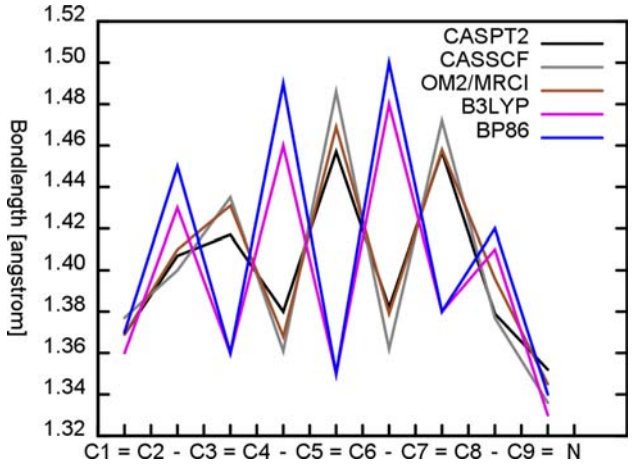

Fig. 3 S_1 bond lengths (Å) of the PSB5 model chromophore. CASPT2 values from Page and Olivucci [62]

Although Hayashi et al. [61] provides an important step towards the understanding of the bR photodynamics, it also shows the limit of current CASSCF technology: due to the factorial scaling of computational cost with the number of correlated electrons, surface hopping simulations of the full chromophore will be prohibited also in the future. In order to overcome this problem, we are working on a QM/MM surface hopping scheme based on the OM2/MRCI method. The latter has been proven to deliver quantitatively satisfying results in the context of color tuning [24, 35]. First results, obtained with analytical excited-state gradient and nonadiabatic coupling vector, are promising. One key test is the geometry of the planar S_1 minimum, Fig. 3 shows the bond-length pattern for the PSB5 model of retinal. As for the energetics, the agreement of the geometry with the CASPT2-optimized reference structure [62] is better than at the CASSCF level of theory. This opens the perspective for exploring the factors that determine efficiency and selectivity of the photoreaction and the suppression of alternative decay channels in retinal proteins, on a quantitative level, on which calculation and experiment are directly comparable.

References

1. Logunov SL, Song L, El-Sayed MA (1996) J Phys Chem 100:18586
2. Kochendoerfer GG, Lin SW, Sakmar TT, Mathies RA (1999). TIBS 24:300
3. Nakanishi K, Balogh-Nair Y, Arnaboldi M, Tsujimoto K, Honig B (1980) J Am Chem Soc 102:7945
4. Van der Steen R, Biesheuvel BL, Lugtenburg J (1986) J Am Chem Soc 108:6410
5. Harbison GS, Mulder PPJ, Pardoen JA (1985) Biochemistry 24:6955
6. Harbison GS, Mulder PPJ, Pardoen JA (1985) J Am Chem Soc 107:4810
7. Wada M, Sakutai M, Inoue Y, Tamura Y, Watanabe Y (1994) J Am Chem Soc 116:1537
8. Kakitani H, Kakitani T, Rodman H, Honig B (1985) Photochem Photobiol 41:471
9. Kochendoerfer G, Wang Z, Oprian DD, Mathies RA (1997) Biochemistry 36:6577
10. Irving CS, Byers GW, Leermake PA (1969) J Am Chem Soc 91:2141
11. Irving CS, Byers GW, Leermake PA (1970) Biochemistry 9:858
12. Beppu Y, Kakitani T (1994) Photochem Photobiol 59:660
13. Birge RR, Murray LM, Pierce BM, Akita H, Balogh-Nair V, Findsen LA, Nakanishi K (1985) Proc Natl Acad Sci USA 82:4117
14. Baasov T, Friedman N, Sheves M (1987) Biochemistry 26:3210
15. Hu J, Griffin RG, Herzfeld J (1994) Proc Natl Acad Sci USA 91:8880
16. Ren L, Martin CH, Wise KJ, Gillespie NB, Luecke H, Lanyi JK, Spudich JL, Birge RR (2001) Biochemistry 40:13906
17. Rajamani R, Gao J (2002) J Comp Chem 23(1):96
18. Dinner AR, Lopez X, Karplus M (2003) Theor Chem Acc 109:118
19. Vreven T, Morokuma K (2003) Theor Chem Acc 109:125
20. Hayashi S, Ohmine I (2000) J Phys Chem B 104:10678
21. Houjou H, Koyama K, Wada M, Sameshima K, Inoue Y, Sakurai M (1998) Chem Phys Lett 294:162
22. Warshel A, Chu ZT (2001) J Phys Chem B 105:9857
23. Zhou H, Tajkhorshid E, Frauenheim Th, Suhai S, Elstner M (2002) Chem Phys 277:91
24. Wanko M, Hoffmann M, Strodel P, Koslowski A, Thiel W, Neese F, Frauenheim T, Elstner M (2005) J Phys Chem B 109:3606
25. Elstner M, Porezag D, Jungnickel G, Elsner J, Haugk M, Frauenheim Th, Suhai S, Seifert G (1998) Phys Rev B 58:7260
26. Okada T, Sugihara M, Bondar A, Elstner M, Entel P, Buss V (2004) J Mol Biol 342:571
27. Champagne B, Perpète EA, Jacquemin D, van Gisbergen SJA, Baerends E-J, Soubra-Ghaoui C, Robins KA, Kirtman B (2000) J Phys Chem A 104(20):4755
28. Van Gisbergen SJA, Fonseca Guerra C, Baerends EJ (2000) J Comp Chem 21(16):1511
29. Martin JML (1996) Chem Phys Lett 259(3):669
30. N. Bondar et al. (2007) (to be published)
31. Bondar A, Fischer S, Smith JC, Elstner M, Suhai S (2004) J Am Chem Soc 126:14668
32. Bondar A, Elstner M, Suhai S, Smith JC, Fischer S (2004) Structure 12:1281
33. Koslowski A, Beck ME, Thiel W (2003) J Comput Chem 24:714
34. Neese F (2003) J Chem Phys 119:9428
35. Hoffmann M, Wanko M, Strodel P, König PH, Frauenheim T, Schulten K, Thiel W, Tajkhorshid E, Elstner M (2006) J Am Chem Soc 128:10808
36. Birge RR, Zhang C (1990) J Chem Phys 92:7178
37. Chizhov I, Schmies G, Seidel R, Sydor JR, Lüttenberg B, Engelhard M (1998) Biophys J 75:999
38. Shimono K, Iwamoto M, Sumi M, Kamo N (2000) Photochem Photobiol 72:141
39. Shimono K, Kitami M, Iwamoto M, Kamo N (2000) Biophys Chem 87:225
40. Shimono K, Furutani Y, Kandori H, Kamo N (2002) Biochemistry 41:6504

41. Shimono K, Iwamoto M, Sumi M, Kamo N (2001) Biochim Biophys Acta 1515:92
42. Shimono K, Hayashi T, Ikeura Y, Sudo Y, Iwamoto M, Kamo N (2003) J Biol Chem 278:23882
43. Kandori H, Furutani Y, Shimono K, Shichida Y, Kamo N (2001) Biochemistry 40:15693
44. Houjou H, Inoue Y, Sakurai M (2001) J Phys Chem B 105:867
45. Wang Q, Schoenlein RW, Peteanu LA, Mathies RA, Shank CV (1994) Science 266:422
46. Atkinson GH, Ujj L, Zhou YD (2000) J Phys Chem A 104:413
47. Herbst J, Heyne K, Diller R (2002) Science 294:822
48. Terentis AC, Zhou Y, Atkinson GH (2003) J Phys Chem A 107:10787
49. Schenkl S, van Mourik F, Friedman N, Sheves M, Schlesinger R, Haacke S, Chergui M (2006) Proc Natl Acad Sci USA 103(11):4101
50. Wanko M, Garavelli M, Bernardi F, Niehaus TA, Frauenheim Th, Elstner M (2004) J Chem Phys 120:1674
51. Garavelli M, Celani P, Bernardi F, Robb MA, Olivucci M (1997) J Am Chem Soc 119:6891
52. Vreven T, Bernardi F, Garavelli M, Olivucci M, Robb MA, Schlegel HB (1997) J Am Chem Soc 119:12687
53. Cembran A, Bernardi F, Olivucci M, Garavelli M (2003) J Am Chem Soc 125:12509
54. Cembran A, Bernardi F, Olivucci M, Garavelli M (2005) Proc Natl Acad Sci USA 102(18):6255
55. Garavelli M, Vreven T, Celani P, Bernardi F, Robb M, Olivucci M (1998) J Am Chem Soc 120:1285
56. Garavelli M, Bernardi F, Robb MA, Olivucci M (1999) J Mol Struct 463:59
57. Tsiper EV, Chernyak V, Tretiak S, Mukamel S (1999) J Chem Phys 110(17):8328
58. González-Luque R, Garavelli M, Bernardi F, Merchán M, Robb MA, Olivucci M (2000) Proc Natl Acad Sci USA 97(17):9379
59. Migani A, Robb MA, Olivucci M (2003) J Am Chem Soc 125:2804
60. Weingart O, Migani A, Olivucci M, Robb MA, Buss V, Hunt P (2004) J Phys Chem A 108:4685
61. Hayashi S, Tajkhorshid E, Schulten K (2003) Biophys J 85:1440
62. Page CS, Olivucci M (2003) J Comput Chem 24:298